MATERIALS CHEMISTRY FRONTIERS

REVIEW

View Article Online
View Journal | View Issue



Cite this: *Mater. Chem. Front.*, 2024, **8**, 341

# Coupling electrochemical $CO_2$ reduction with value-added anodic oxidation reactions: progress and challenges

Yu Li and Tong-Bu Lu *

Received 1st June 2023,
Accepted 8th October 2023

DOI: 10.1039/d3qm00625e

rsc.li/frontiers-materials

Converting $CO_2$ into chemicals using renewable electricity provides a promising avenue to realize carbon neutrality. Substituting the anodic oxygen evolution reaction by thermodynamically more favourable oxidation reactions with value-added products can significantly lower the cell voltage and enhance the output value of overall $CO_2$ electrolysis. In this review, we summarize the up-to-date breakthroughs in electrochemical systems featuring the $CO_2$ reduction reaction ($CO_2$RR) coupled with various anodic oxidation reactions. Moreover, major challenges with possible solutions and future prospects in this field are pointed out, which are expected to benefit researchers and propel this coupling strategy to industrial applications.



## 1. Introduction

The global environmental issues and energy crisis are driving us to substitute traditional fossil fuels with green energy sources. Among the various emerging techniques, electrochemically converting $CO_2$ into value-added feedstocks can not only store renewable electricity in chemical bonds but also promote the natural carbon cycle, and therefore holds potential for realizing carbon-neutrality. Currently, great efforts have been devoted to developing efficient catalysts with excellent Faradaic efficiency (FE), high current density, and low overpotential for the electrochemical $CO_2$ reduction reaction ($CO_2$RR).[1–4] However, although remarkable catalysts with near-unity FEs and close-to-zero overpotentials have emerged, energy utilization is still far from satisfactory considering the whole electrolysis. For instance, according to the Hess law, the energy consumption for $CO_2$ reduction to CO/HCOOH only takes a small part in the overall $CO_2$ electrolysis where the oxygen evolution reaction (OER) with a theoretical potential of 1.23 V *versus* reversible hydrogen electrode (*vs.* RHE) is usually adopted as the anodic reaction.

Cathode:

$$CO_2(g) + H_2(g) \rightarrow CO(g) + H_2O(l)$$
$$(\Delta G^\circ = 20.1\ \text{kJ mol}^{-1};\ E^0 = -0.106\ \text{V}) \quad (1)$$

$$CO_2(g) + H_2(g) \rightarrow HCOOH(l)$$
$$(\Delta G^\circ = 33.0\ \text{kJ mol}^{-1};\ E^0 = -0.199\ \text{V}) \quad (2)$$

Anode:

$$H_2O(l) \rightarrow H_2(g) + 1/2O_2(g)$$
$$(\Delta G^\circ = 237.1\ \text{kJ mol}^{-1};\ E^0 = 1.23\ \text{V}) \quad (3)$$

Overall:

$$CO_2(g) \rightarrow CO(g) + 1/2O_2(g)$$
$$(\Delta G^\circ = 257.2\ \text{kJ mol}^{-1};\ E^0 = 1.34\ \text{V}) \quad (4)$$

$$CO_2(g) + H_2O(l) \rightarrow HCOOH(g) + 1/2O_2(g)$$
$$(\Delta G^\circ = 270.1\ \text{kJ mol}^{-1};\ E^0 = 1.43\ \text{V}) \quad (5)$$

Intuitively, the cathodic reduction of $CO_2$ to CO and HCOOH only takes 7.81% and 12.2% of the total energy consumption for overall $CO_2$ electrolysis, respectively, whereas the anodic OER consumes the vast majority of the electricity. In addition, the anodic product $O_2$ is of little value. To increase the energy utilization efficiency, many alternative reactions have been employed to replace the unsatisfactory OER (Table 1).[5–9] Briefly, these reactions can be divided into three categories (Fig. 1). The first category includes reactions thermodynamically more favourable than the OER that can effectively reduce the cell voltage. For example, ammonia, urea and hydrazine oxidation reactions (denoted as the AOR, UOR, and HzOR, respectively) have been substituted for the OER in water splitting owing to their significantly lower theoretical potentials (0.06, 0.37 and

*MOE International Joint Laboratory of Materials Microstructure, Institute for New Energy Materials and Low Carbon Technologies, School of Materials Science & Engineering, Tianjin University of Technology, Tianjin 300384, China.*
*E-mail: lutongbu@tjut.edu.cn*

Table 1 Alternative anodic oxidation reactions for the OER in $CO_2$ overall electrolysis

| | Anodic oxidation reaction | Redox potential (V *vs.* RHE) |
|---|---|---|
| OER | $H_2O \rightarrow O_2 + 4H^+ + 4e^-$ | 1.23 |
| Category I | $2NH_3 + 6OH^- \rightarrow N_2 + 6H_2O + 6e^-$ | 0.06 |
| | $CO(NH_2)_2 + 6OH^- \rightarrow CO_2 + N_2 + 5H_2O + 6e^-$ | 0.07 |
| | $N_2H_4 + 4OH^- \rightarrow N_2 + 4H_2O + 4e^-$ | −0.33 |
| Category II | $2Cl^- \rightarrow Cl_2 + 2e^-$ | 1.36 |
| | $2H_2O \rightarrow H_2O_2 + 2H^+ + 2e^-$ | 1.76 |
| Category III | $CH_3OH + 3OH^- \rightarrow HCOO^- + 3H_2O + 2e^-$ | 0.11 |
| | $C_3H_8O_3 + 11OH^- \rightarrow 3HCOO^- + 8H_2O + 8e^-$ | 0.14 |
| | $C_6H_{12}O_6 + 2OH^- \rightarrow C_6H_{12}O_7 + H_2O + 2e^-$ | 0.90 |
| | $C_6H_6O_3 + 6OH^- \rightarrow C_6H_2O_5^{2-} + 4H_2O + 4e^-$ | 0.30 |
| | $S^{2-} \rightarrow S + 2e^-$ | −0.48 |
| | $2HS^- + 2OH^- \rightarrow S_2^{2-} + 2H_2O + 2e^-$ | 0.14 |

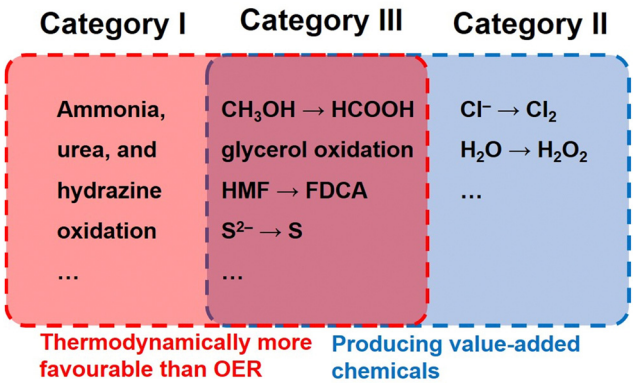


Fig. 1 Different categories of alternative anodic oxidation reactions.

−0.33 V *vs.* RHE for the AOR, UOR, and HzOR, respectively) to markedly cut down the applied cell voltage.[10–12] Although no value-added products are obtained, these sacrificial agent-like oxidation reactions can be adopted to eliminate pollutants in waste water.[13,14]

Oxidation reactions featuring no superior theoretical potential but value-added products (Category II) have also been employed as the anodic side of full electrolysis. A representative is water oxidation to $H_2O_2$ ($2H_2O \rightarrow H_2O_2 + 2H^+ + 2e^-$, $E^0$ = 1.76 V *vs.* RHE). Albeit this two-electron process requires a higher potential by 0.53 V than that of the OER, the price of $H_2O_2$ (~$560 per ton) is about 14 times as high as that of $O_2$ (~$40 per ton), making this substitution economically viable.[5] As the most attractive substitutions for the OER, selective oxidation of small organic molecules such as alcohols, aldehydes, and amines (Category III) enables simultaneous voltage reduction and value-added chemical production.[15–20] The market prices of the raw materials and products for these alternative oxidation reactions are summarized in Table 2.[5] Evidently, the added values and the electricity output (added value per electron) for the alternative oxidation reactions are all times higher than that for the OER. In particular, the conversion of 5-hydroxymethylfurfural (HMF) to 2,5-furandicarboxylic acid (FDCA) holds the highest added value of up to $30970 per ton, suggesting its tremendous superiority compared with the OER.

Currently, increasing efforts are being devoted to coupling the above reactions with the $CO_2$RR to fabricate an energy-efficient full electrolyser. Although several reviews on alternative anodic reactions coupled with the hydrogen evolution reaction (HER) have been reported, the case is much different in $CO_2$ electrolysis considering the electrolyte choice, mass transfer, electrode design, cell structure, *etc.*[21–23] This review starts with a brief introduction of different types of anodic oxidation reactions. Subsequently, we will present up-to-date progress in alternative anodic reactions that have already been or hold the potential to be applied in $CO_2$RR coupling systems, with elucidation of the structure–performance relationship. Finally, we will systematically discuss the challenges and prospects for $CO_2$RR coupling systems regarding the design of electrocatalysts and electrolysers for guidance on propelling this technique towards industrial applications.

## 2. Recent advances in coupling the $CO_2$RR with alternative anodic reactions

### 2.1. Category I

N-containing species such as ammonia and urea are major pollutants in industrial and agricultural wastewater, the excessive emission of which will not only lead to the eutrophication

Table 2 Economic comparison between the OER and alternative oxidation reactions

| Raw material | Market price of the raw material ($ per ton) | Product | Market price of the product ($ per ton) | Added value ($ per ton) | Added value per electron ($ per (ton e)) |
|---|---|---|---|---|---|
| $H_2O$ | 0.6 | $O_2$ | 40 | 39.4 | 9.8 |
| $H_2O$ | 0.6 | $H_2O_2$ | 560 | 559.4 | 279.7 |
| NaCl | 68 | $Cl_2$ | 822 | 754 | 377 |
| $CH_3OH$ | 340 | HCOOH | 970 | 630 | 157.5 |
| $CH_3CH_2OH$ | 610 | $CH_3COOH$ | 680 | 70 | 17.5 |
| $C_3H_8O_3$ (glycerol) | 970 | $C_3H_6O_3$ (lactic acid) | 1580 | 610 | 305 |
| $C_5H_4O_2$ (furfural) | 1170 | $C_5H_4O_3$ (2-furoic acid) | 6230 | 5060 | 2530 |
| $C_6H_6O_3$ (5-Hydroxymethylfurfural) | 1030 | $C_6H_4O_5$ (2,5-Furandicarboxylic acid) | 32000 | 30970 | 5161.7 |
| $C_6H_{12}O_6$ (glucose) | 315 | $C_6H_{12}O_7$ (gluconic acid) | 644 | 329 | 164.5 |

 

of water and destroy the river and lake ecosystems, but also threaten drinking water safety. Classical methods to decompose these pollutants are based on chemical oxidation reactions using toxic and hazardous reagents, which are not preferred given the increasing environmental and economic requirements. Electrochemical oxidation of N-containing pollutants provides appealing routes to remedy the above issues. The pollutants can be transformed directly by current on the electrode surface or indirectly by active radicals *in situ* generated during electrolysis, rather than hazardous chemicals. However, in spite of their low theoretical potentials, both the AOR and UOR involve $6e^-$-transfer processes ($2NH_3 + 6OH^- \rightarrow N_2 + 6H_2O + 6e^-$; $CO(NH_2)_2 + 6OH^- \rightarrow CO_2 + N_2 + 5H_2O + 6e^-$), and thus suffer from sluggish kinetics. Accordingly, developing highly efficient catalysts is essential for the energy-efficient $CO_2$RR-AOR and $CO_2$RR-UOR couple at an industrial current density ($>100$ mA cm$^{-2}$).

According to the dehydrogenation degree of N intermediates in the N–N coupling step, there are two possible pathways for AOR: (1) the adsorbed ammonia undergoes continuous dehydrogenation steps and the N–N coupling step occurs between two *N species; (2) the N–N coupling step occurs between two incomplete dehydrogenated *$NH_x$ species followed by further dehydrogenation of *$N_2H_y$ species ($x$ = 1–3 and $y$ = 2–5).[24–26] Pt-based catalysts have shown excellent activity in the AOR. The introduction of Ir and Ni into the Pt lattice can decrease the energy barrier of dehydrogenation of *$NH_2$ to *NH and the rate-determining step (RDS) on the Pt surface *via* elevating the d-band centre for enhanced *NH adsorption, thereby accelerating the reaction kinetics and reducing the overpotential.[25,26] Recently, Ni catalysts have been investigated for the cost-effective AOR. Xu *et al.* reported a bimetallic NiCu catalyst that could achieve 80% removal of ammonia in 500 ppm $NH_3$ solution.[27] Almomani *et al.* reported that an *in situ* formed $Ni(OH)_2$ layer over NiO endowed the NiO-$TiO_2$ composite catalyst with over 90% removal of N in wastewater with a low ammonia concentration of $<100$ ppm.[28]

Although inspiring progress has been made in the AOR, the development of $CO_2$RR-AOR full electrolysis remains immature. Klinkova's group evaluated the $CO_2$RR-AOR couple featuring an Ag/C cathode and Pt/C anode in an H-type cell.[29] Compared with the $CO_2$RR-OER, the cell voltage decreased by 0.78 V at a current density ($j$) of 0.1 mA cm$^{-2}$ with the addition of 1 M ammonia in the anolyte. However, the improvement shrank to 0.32 V when $j$ was increased to 10 mA cm$^{-2}$. Besides, the Pt/C catalyst got poisoned easily due to the overstrong adsorption of *N-species, and showed no activity towards the AOR after a four-hour test.

As shown above, in addition to the low solubility of $CO_2$ in aqueous solution ($\sim$34 mM under ambient conditions), the poor mass transfer efficiency over both the anode and the cathode in commonly used H-type cells heavily hindered the electrocatalytic performance of the $CO_2$RR-AOR couple. To overcome the mass transfer limitation, a flow cell with a cathodic gas diffusion electrode (GDE) was fabricated. Both the anolyte and catholyte flow in the flow field immediately remove the products and refresh the electrolyte near the electrode, thereby exposing active sites with a high-concentration of local ammonia and $CO_2$. Moreover, the cathodic GDE helps to construct a three-phase interface composed of electrode-water-$CO_2$, which prominently enhances the contact between the catalyst and $CO_2$ and thus boosts the current density (a more detailed discussion is presented in Section 3.2). Choi *et al.* successfully coupled the $CO_2$RR with the AOR in a closely packed gas diffusion electrolyser consisting of a Au cathode and a Pt/C anode (Fig. 2a).[30] The cell voltages of the $CO_2$RR-OER and $CO_2$RR-AOR were 3.0 and 2.0 V at 10 mA cm$^{-2}$, respectively, and the disparity increased to 1.5 V at 50 mA cm$^{-2}$, demonstrating the boosted energy efficiency for the $CO_2$RR-AOR couple in a gas diffusion electrolyser (Fig. 2b). Moreover, the $H_2$/CO ratio of the cathodic product syngas could be optimized by changing the $NH_3$ concentration in the anolyte (Fig. 2c). However, a similar activity decrease was also observed for anodic Pt/C in this work. In addition, it should be pointed out that these reported $CO_2$RR-AOR couples require an extremely high concentration of ammonia to markedly reduce the full cell voltage, whereas the concentration of $NH_3$ (calculated by N mass) in domestic or agricultural effluents is usually below 100 mg L$^{-1}$, equal to approximately 7 mM $NH_3$, which means that extra $NH_3$ enrichment procedures are demanded for the wastewater before being applied in the $CO_2$RR-AOR couple. Therefore, highly active catalysts that can efficiently convert low concentrations of $NH_3$ with a prolonged lifetime are crucial for the utilization of the $CO_2$RR-AOR technique.

For the UOR, apart from the dehydrogenation N–N coupling steps, it also involves the breakage of the C–N bond before the formation of $N_2$.[31] Jiang *et al.* found that on O-incorporated NiMoP nanotube arrays, the last dehydrogenation step from *CONHN to *$CON_2$ and subsequent C–N dissociation of *$CON_2$ into *CO and $N_2$ were the slow steps for the UOR, whereas the

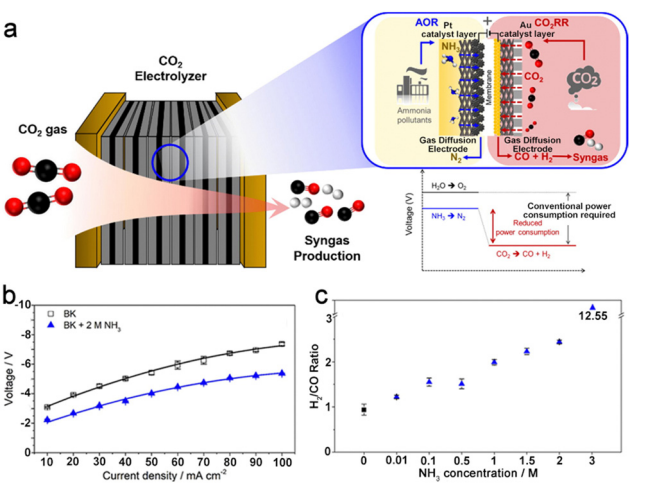


Fig. 2 (a) Schematic illustration of the $CO_2$RR-AOR couple in a gas diffusion electrolyser. (b) Voltages at different current densities in 0.5 M $KHCO_3$ (BK) or 0.5 M $KHCO_3$ + 2 M $NH_3$ (BK + 2 M $NH_3$). (c) $H_2$/CO ratio of syngas as a function of the $NH_3$ concentration at 10 mA cm$^{-2}$. Reproduced with permission from ref. 30. Copyright 2022, Elsevier Ltd.

other steps were all spontaneous.[12] In an electrolyte containing 1.0 M KOH + 0.5 M urea, a potential of merely 1.41 V *vs.* RHE was required to deliver a *j* value of 100 mA $cm^{-2}$, 340 mV lower than that of the OER, indicating the improved energy efficiency for the UOR. Besides, the result of long-term electrolysis revealed that the current density slightly dropped from 20 to 17.5 mA $cm^{-2}$ after 40 h of the UOR, implying the fine stability of the catalyst. Recently, Clark *et al.* investigated the feasibility of coupling the $CO_2$RR with the UOR using Sn wire and a NiFe film as corresponding electrodes.[32] The voltage of the full electrolyser was reduced by the addition of 0.25 M urea in the anolyte, and the FE of the $CO_2$RR was even slightly higher than that of $CO_2$ coupled with the OER.

Hydrazine is also a pollutant in wastewater, and many efforts have been devoted to the development of efficient HzOR catalysts. HzOR involves 4-$e^-$ transfer with extremely low theoretical potential ($N_2H_4 + 4OH^- \rightarrow N_2 + 4H_2O + 4e^-$; $E^0$ = −0.33 V *vs.* RHE), which is beneficial to reduce the full cell voltage when employed as the anode reaction. Zhu *et al.* fabricated a Ni/C hybrid nanosheet array catalyst for efficient HzOR.[10] DFT calculation results revealed that the Ni sites in the hybrid catalyst favoured the dehydrogenation of $N_2H_4$ to $N_2$, thereby enhancing the HzOR performance. Shi's group reported an unusual HzOR pathway on the CoP/NiCoP heterogenous interface featuring the cleavage of the N–N bond before dehydrogenation with a reduced energy barrier.[11] As a result, a potential of merely 0.09 V *vs.* RHE was required to deliver 200 mA $cm^{-2}$ current density for HzOR by the optimized catalyst in 1.0 M KOH + 0.1 M $N_2H_4$, 1.54 V lower than that for OER by $RuO_2$. However, the $CO_2$RR-HzOR couple has not been reported, to our knowledge. In fact, we can only find limited literature that has reported the successful coupling of the $CO_2$RR with the above water pollutant degradation reactions, whereas the latter have already been employed to couple with the hydrogen evolution reaction (HER). The main reason is that the $CO_2$RR performance is closely influenced by the catalyst activity, gas–liquid–solid interfacial mass transfer, electrolyte types, *etc.*, much more complicated than the case of water splitting. Moreover, the requirement of high concentrations of pollutants to significantly reduce the full cell voltage leads to extra energy-consuming preconcentration of wastewater. Accordingly, further techno-economic analysis is required to evaluate the coupling of the $CO_2$RR with Category I reactions, and developing highly active catalysts that can deal with low concentrations (ppm level) of pollutants may address the issue.

### 2.2. Category II

The chlorine oxidation reaction (COR) is one of the most crucial chemical industrial techniques as the products $Cl_2$ and $ClO^-$ are important feedstocks in the pharmacy, disinfection, and rubber industries. Coupling $CO_2$ reduction to CO with the COR enables simultaneous production of CO, $KHCO_3$, and $Cl_2$ with 100% atom economy theoretically ($3CO_2 + 2KCl + H_2O \rightarrow CO + 2KHCO_3 + Cl_2$). For example, Guo *et al.* have successfully assembled a carbon black supported Ni catalyst cathode and

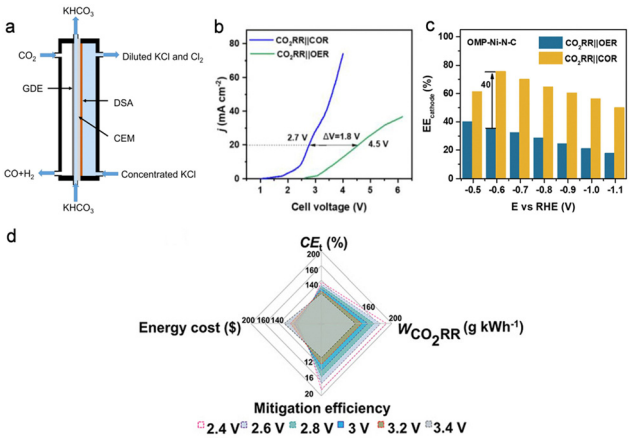


Fig. 3 (a) Schematic illustration of the flow cell for the $CO_2$RR-COR couple. Reproduced with permission from ref. 33. Copyright 2020, Elsevier Ltd. (b) Linear sweep voltammetry curves and (c) cathode energy efficiencies for the $CO_2$RR coupled with the COR or OER. Reproduced with permission from ref. 34. Copyright 2022, Elsevier Ltd. (d) $CO_2$ emission and economy evaluation *via* total cell efficiency, mitigation efficiency, the weight of $CO_2$ reduced per kWh electricity consumption, and energy cost on the basis of per kWh electricity consumption for the $CO_2$RR-COR couple in seawater. Reproduced with permission from ref. 35. Copyright 2021, John Wiley & Sons, Inc.

commercial dimensional stable anode in a gas diffusion electrolyser for the efficient $CO_2$RR-COR (Fig. 3a).[33] High FEs of up to 98.5% and 75.2% were achieved at 250 mA $cm^{-2}$ for $CO_2$RR-to-CO and COR-to-$Cl_2$, respectively. Lu's group introduced ordered mesoporous structures into cathodic Ni–N–C and anodic $Co_3O_4$ catalysts to enhance the activity of the $CO_2$RR-COR couple.[34] The improved mass transfer owing to the ordered mesoporous structure effectively boosted the current density. Moreover, the cell voltage was sharply reduced from 4.5 to 2.7 V to achieve 20 mA $cm^{-2}$ with the substitution of the OER with the COR (Fig. 3b), and the energy efficiency (EE) for the cathode was increased by 40% (Fig. 3c). Qiu's group have evaluated the economy and the net reduction of $CO_2$ for the $CO_2$RR-COR using seawater as the electrolyte, and the results suggested a total cell efficiency for producing CO and $Cl_2$ exceeding 100% without extra $CO_2$ emission (Fig. 3d).[35] The above work demonstrates the huge potential and viability of the s$CO_2$RR-COR couple in the industrial process.

$H_2O$ oxidation to $H_2O_2$ rather than $O_2$ is attracting increasing interest. Although the theoretical potential for $H_2O_2$ formation (1.76 V *vs.* RHE) is higher than that of $O_2$ (1.23 V *vs.* RHE), 2-$e^-$ transfer of the $H_2O_2$ evolution reaction makes it more dynamically favoured than the OER. However, no work has been reported focused on coupling the $CO_2$RR with the $H_2O_2$ evolution reaction to date. The Wang group found a $CO_2$/carbonate mediated electrochemical $H_2O$ oxidation for high-performance $H_2O_2$ production.[36] The carbonate ions could steer the 4-$e^-$ pathway to 2-$e^-$ through carbonate radicals and percarbonate intermediates. Consequently, an industrial scale current density of up to 1.3 A $cm^{-2}$ was achieved with an $H_2O_2$ FE of 70% in the $K_2CO_3$ electrolyte. This inspiring result

 

indicates the possibility of coupling the $CO_2RR$ with $H_2O$ oxidation to $H_2O_2$ in the anion exchange membrane (AEM) electrolyser where *in situ* formed $CO_3^{2-}$ in the cathode can migrate to the anode to help boost the formation of $H_2O_2$.

### 2.3. Category III

Methanol is a main product in methane conversion and an important building block for the chemical industry. Selective oxidation of methanol to formic acid (formate) is desired given the large disparity in prices of methanol (~$200 per ton) and formic acid (~$600 per ton). Wei *et al.* fabricated CuO nanosheets on Cu foam for the efficient methanol oxidation reaction (MOR) (Fig. 4a).[16] A high $FE_{formate}$ of up to 95% was achieved for the MOR, and the potential was decreased by 250 mV to achieve a current density of 10 mA $cm^{-2}$ compared with that for the OER. Besides, mesoporous $SnO_2$ on carbon cloth was prepared for the efficient $CO_2RR$ with 81% $FE_{formate}$. For the $CO_2RR$-MOR couple, it required only 0.93 V to deliver a current density of 10 mA $cm^{-2}$, which was 500 mV lower than that for the $CO_2RR$-OER. Another work by Cao *et al.* presented a $CO_2RR$-MOR full electrolyser equipped with Bi- and Ni-metal–organic framework-derived catalysts as the respective cathode and anode.[17] A current density of 27 mA $cm^{-2}$ was achieved at a cell voltage of 3.0 V with a $FE_{formate}$ of ~100% at both electrodes (Fig. 4b). Lan's group successfully integrated metalloporphyrin (Ni) and $Ni_8$ clusters in PCN-601 as a bifunctional electrocatalyst for the $CO_2RR$-MOR couple.[37] The Ni site in metalloporphyrin served as the active centre for the $CO_2RR$ to CO, while the $Ni_8$ cluster acted as the site for the MOR to formate. Consequently, high $FE_{CO}$ and $FE_{formate}$ values of over 90% were obtained at 2.2 V with a current density of 7 mA $cm^{-2}$. Nevertheless, the current densities above are too low to meet industrial requirements. Recently, our group developed a bifunctional CuSn alloy electrocatalyst with a hierarchical structure for the $CO_2RR$-MOR couple at a high current density.[15] In an H-type cell, the $CO_2RR$-MOR couple delivered a current density as high as 125 mA $cm^{-2}$ with near-unity $FE_{formate}$ at both sides, corresponding to a formate production rate of up to 3313 μmol $h^{-1}$ $cm^{-2}$. Such a strategy contributed to a reduction in energy consumption by 40% for formate synthesis. Moreover, *in situ* Raman spectroscopic results revealed that the $CH_3OH$ adsorbed on the catalyst surface *via* an O atom followed by a series of dehydrogenation steps to form an *OCH intermediate. Subsequently, *OCHO was generated through the addition of an O atom from the OH group to *OCH and then desorbed from the CuSn alloy surface for formate formation (Fig. 4c and d). This reaction pathway was also verified on partially pyrolyzed Ni–organic frameworks.[18] The *in situ* formed NiOOH sites were conducive to O–H activation and thus promote the oxidation of methanol to formate. In a zero-gap membrane electrode assembly (MEA), the $CO_2RR$-MOR couple exhibited an excellent performance of ~500 mA $cm^{-2}$ at 2.2 V with over 90% FEs for both $CO_2RR$-to-CO and MOR-to-formate, ranking top among the up-to-date $CO_2RR$-MOR systems (Fig. 4e and f).

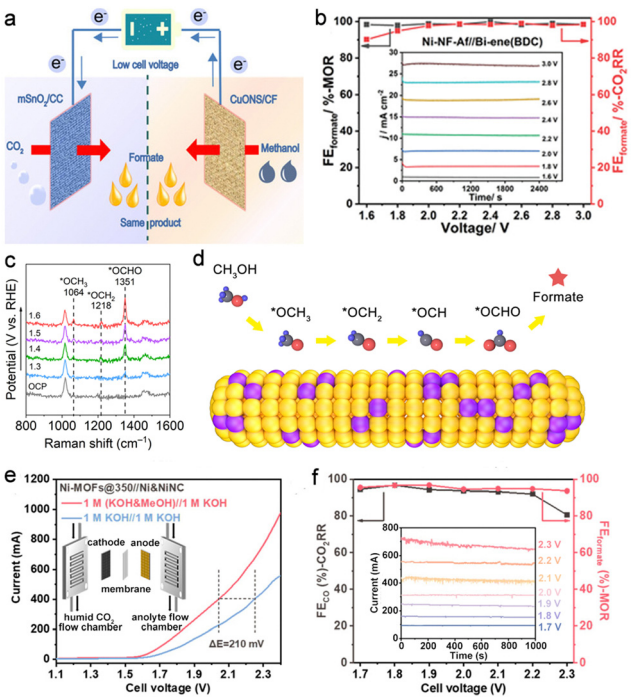


Fig. 4 (a) Schematic illustration of the $CO_2RR$-MOR couple. Reproduced with permission from ref. 16. Copyright 2020, John Wiley & Sons, Inc. (b) Cathodic and anodic $FE_{formate}$ of the $CO_2RR$-MOR couple using Bi- and Ni-MOF-derived materials as corresponding electrodes. Reproduced with permission from ref. 17. Copyright 2021, John Wiley & Sons, Inc. (c) *In situ* Raman spectra and the (d) proposed reaction pathway for the MOR on CuSn alloy. Reproduced with permission from ref. 15. Copyright 2022, Elsevier Ltd. (e) Polarization curves (inset shows the MEA scheme) and (f) voltage-dependent FE (inset shows the corresponding *i*-*t* curves) for the $CO_2RR$-MOR in an MEA electrolyser. Reproduced with permission from ref. 18. Copyright 2023, American Chemical Society.

Electrochemical upgrade of biomass-derived materials such as glycerol, furfurals and glucose into useful chemicals is thermodynamically more favourable than the OER owing to the –CHO and –OH groups. Glycerol is a massive byproduct of the transesterification process for biodiesel and soap production, and it is profitable to upgrade glycerol into other chemicals through the glycerol oxidation reaction (GOR). Verma *et al.* performed a techno-economic analysis of cradle-to-gate $CO_2$ emissions of the overall $CO_2RR$ process using grid electricity, and the result indicated that only HCOOH could be produced in a carbon-neutral or -negative manner when the OER was employed as the anodic reaction.[38] As a step further, they found that using the GOR on Pt black at the anode lowered the onset potential for the overall $CO_2$ electrolysis by 0.85 V, contributing to an energy consumption reduction of 53%, which drastically reduced the operating costs and carbon footprint of $CO_2$ electrolysis and thereby made the production of CO, $C_2H_4$, and $CH_3CH_2OH$ become carbon-neutral, strongly evidencing the economic viability of the $CO_2RR$-GOR couple. However, there are various products for the GOR such as glyceraldehyde, glycerate, lactate, glycolate, formate, and carbonate, resulting in poor selectivity. A flow cell consisting of a Bi/C cathode and Pt/C anode has been reported for coupling the $CO_2RR$ with

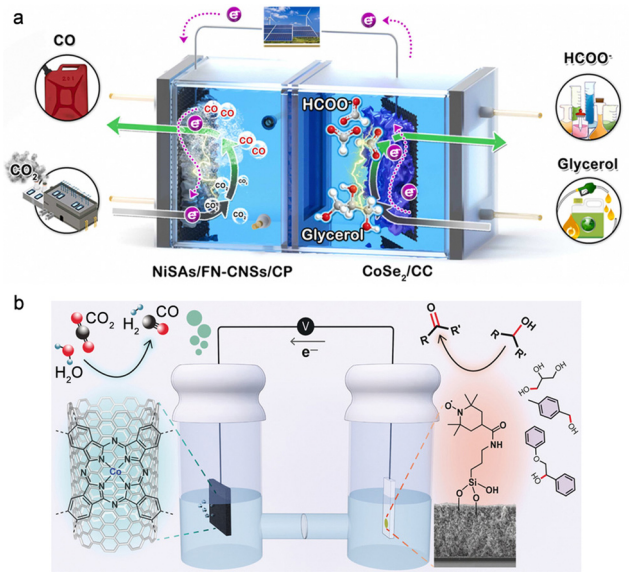


Fig. 5 (a) Schematic illustration of the electrolyser featuring $CO_2$RR-to-CO coupled with GOR-to-formate. Reproduced with permission from ref. 40. Copyright 2022, Elsevier Ltd. (b) Coproduction of syngas and glyceraldehyde using the $CO_2$RR-GOR couple. Reproduced with permission from ref. 41. Copyright 2020, John Wiley & Sons, Inc.

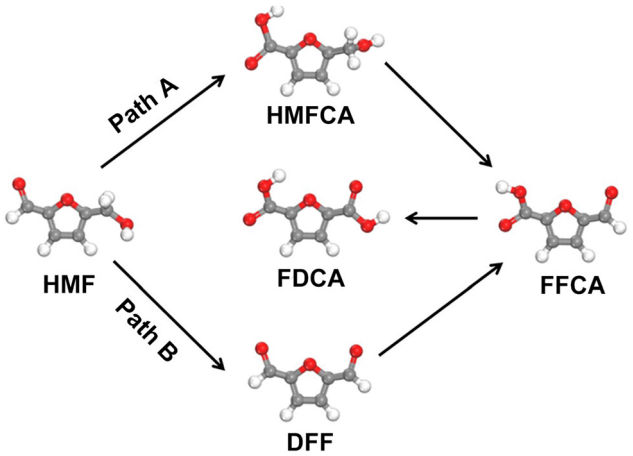


Fig. 6 Reaction pathways for the HMFOR.

the GOR.[39] While a high formate concentration of 18 g $L^{-1}$ was obtained by the cathodic $CO_2$RR with over 80% FE at 200 mA $cm^{-2}$, a low FE of ~20% was delivered for formate by the anodic GOR owing to the severe overoxidation evidenced by the high FE of up to 40% for the carbonate product. Wang *et al.* constructed an F, N co-doped carbon nanosheet-supported Ni single atom cathode and carbon cloth-supported $CoSe_2$ anode to couple the $CO_2$RR with the GOR (Fig. 5a).[40] A long-term continuous electrolysis of 400 h was achieved at 100 mA $cm^{-2}$ with both the cathodic $FE_{CO}$ and anodic $FE_{formate}$ kept over 90%. Apart from formate, another useful chemical glyceraldehyde was selectively generated at the anode of the $CO_2$RR-GOR by Reisner's group.[41] They reported a hybrid assembly based on a (2,2,6,6-tetramethylpiperidin-1-yl)oxyl electrocatalyst modified with a silatrane-anchor for selective glyceraldehyde production from glycerol with an FE of up to 83%; meanwhile, syngas was produced at the cathode using cobalt phthalocyanine on carbon nanotubes as the catalyst (Fig. 5b).

The electrochemical 5-hydroxymethylfurfural (HMF) oxidation reaction (HMFOR) has attracted increasing attention.[42–45] Composed of a –CHO and a $–CH_2OH$ with a furan ring, HMF can be oxidized to 2,5-diformylfuran (DFF) *via* initial $–CH_2OH$ oxidation, or 5-hydroxymethyl-2-furancarboxylic acid (HMFCA) *via* initial –CHO oxidation. Subsequently, the DFF and HMFCA can be further oxidized to 2-formyl-5-furancarboxylic acid (FFCA), and finally to 2,5-furandicarboxylic acid (FDCA) (Fig. 6). The choice of the DFF-pathway or HMFCA-pathway for the oxidation of HMF to FDCA greatly depends on the pH of the electrolyte.[46] Generally, the HMFOR undergoes the HMFCA-path in a strong alkaline electrolyte (pH > 13) due to the preferential adsorption of the aldehyde group on the catalyst, whereas the DFF-pathway is favoured in the electrolyte with pH < 13 where the adsorption of the alcohol group becomes thermodynamically more favourable.[46] To further investigate the HMFOR pathway, Wang's group developed a vibrational spectroscopy technique using *in situ* sum frequency generation to monitor the interfacial process during the HMFOR.[47] A signal related to HMFCA emerged and grew stronger as the electrolysis time was prolonged, which validated the HMFCA-pathway for the HMFOR. To simultaneously promote the oxidation of $–CH_2OH$ and –CHO, Lu *et al.* introduced Ni into the tetrahedral catalytic sites of cobalt spinel oxides.[48] The Ni and Co sites served as active centres for $–CH_2OH$ and –CHO adsorption, respectively, thus enhancing the HMFOR with a high yield of 92.4% and FE of 90.3% for FDCA.

With the remarkable progress made in the HMFOR, however, few works about the $CO_2$RR-HMFOR couple have been reported so far. Recently, Han's group carried out the coupling of the HMFOR with the $CO_2$RR (Fig. 7a and b).[19] The full electrolyser featuring $PdO_x$/ZIF-8 as the cathode and PdO as the anode only required an onset cell voltage of 1.06 V for the $CO_2$RR-HMFOR couple, 0.71 V lower than that of the $CO_2$RR-OER couple (Fig. 7c). Different from previous studies for the HMFOR, an acidic anolyte containing $H_2SO_4$ (0.5 M)/$CH_3CN$ (6.0 M)/$H_2O$ was employed, and the products were mainly maleic acid and formic acid, indicating that a strong acidic environment may lead to an unconventional reaction pathway involving C–C breaking and furan ring opening for the HMFOR. Notably, the organic acid yield reached 84.3% for the HMFOR, including 60.0% formic acid and 24.3% maleic acid, accompanied by a $FE_{CO}$ of 97.0% for the $CO_2$RR at 103.5 mA $cm^{-2}$ (Fig. 7d and e).

There are also some other oxidation reactions that have already been or have the potential to be coupled with the $CO_2$RR. Sulfur production through the sulfide oxidation reaction (SOR) is an appealing candidate for the anodic reaction in overall $CO_2$ electrolysis by virtue of its low potential (0.14 V *vs.* RHE). Besides, the ingredient $H_2S/S^{2-}$ widely exists in industrial exhaust/effluent. Therefore, coupling the $CO_2$RR with the

 

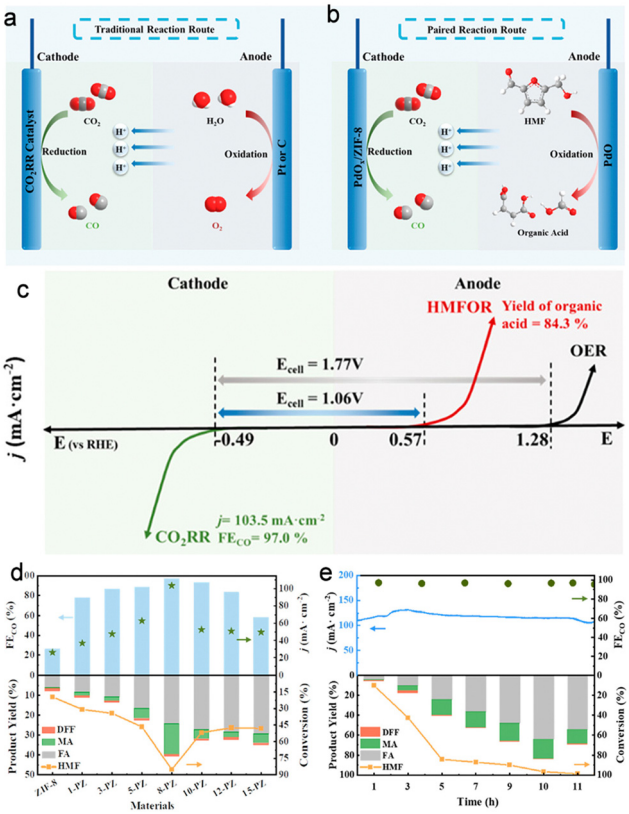


Fig. 7 Overview of (a) $CO_2$RR-OER and (b) $CO_2$RR-HMFOR routes. (c) Comparison between the $CO_2$RR-OER and the $CO_2$RR-HMFOR. (d) $CO_2$RR and HMFOR performances with different anodic catalysts. (e) Long-term electrolysis results of the $CO_2$RR and HMFOR. Reproduced with permission from ref. 19. Copyright 2022, American Chemical Society.

SOR is also of environmental value. Liu's group recently carried out a co-electrolysis system consisting of Bi for $CO_2$RR-to-formate, and S, Cu-codoped cobalt hydroxide for SOR-to-sulfur, which showed a pronounced reduction in energy consumption.[49] To avoid the deposition of S on the anode, an alkaline electrolyte (1 M KOH + 1 M $K_2S$) was employed to generate soluble $S_x^{2-}$ from the direct SOR. As a result, the substitution of the OER with the SOR markedly lowered the cell voltage from 3.43 to 2.10 V at 100 mA $cm^{-2}$, with near-unity faradaic efficiencies for both sides. Economic evaluation based on the cell operation conditions and the prices of cathodic and anodic products revealed a gross margin of \$0.35 kW $h^{-1}$ for the $CO_2$RR-SOR, about 2 times as high as that for the $CO_2$RR-OER (\$0.18 kW $h^{-1}$), further demonstrating the economic viability of the former. Electricity-driven partial oxidation of methane is also a promising anodic reaction of overall $CO_2$ electrolysis.[50,51] Lu *et al.* developed an efficient solid oxide electrolyser for the coupling of $CO_2$ reduction with $CH_4$ oxidation to produce syngas.[52] However, the high operating temperature (1073 K) for $O^{2-}$ transport led to extra energy input. Given the insoluble $CH_4$, the construction of a high-quality gas–liquid–solid interface using gas diffusion electrodes will favour the efficient coupling of the $CO_2$RR with $CH_4$ oxidation. In addition to the aforementioned small molecule oxidation, electrochemical upcycling of plastic waste[53] or reforming of raw biomass such as lignin[54] and chitin[55] are also competing substitutions for the OER. In particular, electrochemical conversions of lignin and chitin have already been successfully employed as the anodic reaction for energy-saving hydrogen evolution systems, demonstrating the possibility for $CO_2$ electrolysis.[55,56] However, achieving high selectivity for the target product remains a huge challenge due to the complicated structures and decomposition pathways for these macromolecules. Moreover, in addition to the electrolysis device design, comprehensive techno-economic analysis covering not only the design of electrolysis devices but also the up- and down-stream supply chain is urgently demanded for guidance on the development of industrial-scale plants.

## 3. Challenges in coupling the $CO_2$RR with alternative anodic reactions

### 3.1. Trade-off between conversion and current density

To reduce the cell voltage and enhance the current density for overall $CO_2$ electrolysis, a high-concentration substrate is usually required on the anodic side. However, the concentration of the substrate decreases as the electrolysis time is prolonged, which leads to a continuous drop in current density. Besides, the faradaic efficiencies of these alternative anodic reactions may also decrease due to the low reactant concentration. To address this issue, one common way is to refresh the anolyte with a high-concentration substrate.[15] However, such a strategy heavily restricts the conversion of the substrate, and brings extra procedures for the separation of products and the unreacted substrate. A more feasible solution is to develop efficient catalysts that are able to selectively convert the substrates at low concentrations. Wang's group fabricated a catalyst featuring dispersed Ru atoms in a Cu nanowire matrix towards efficient $NO_3^-$ reduction to $NH_3$.[57] An industrial-scale current density of up to 1 A $cm^{-2}$ was achieved with an $NH_3$ FE of 93% at a low nitrate concentration of typical industrial wastewater (2000 ppm). More importantly, 99% of the nitrate could be converted to $NH_3$ with the FE maintained over 90% at 400 mA $cm^{-2}$, with the concentration of the nitrate residue as low as 50 ppm. Although this work is focused on the cathodic process, we can learn from it that active sites with a high density (dispersed Ru atoms) and porous structure with a high surface area (hollow Cu nanowire matrix) endow the catalyst with enhanced performance at a low substrate concentration. Besides, increasing the local substrate concentration near the electrode surface with functional groups may also help to maintain the faradaic efficiency and current density when the substrate concentration is reduced. For example, amine groups anchored on the electrode surface can capture dilute $CO_2$ and thus enhance the FE for the $CO_2$RR.[58,59]

### 3.2. Electrolyser design

In addition to electrocatalysts, electrolysers with different architectures also influence the performance of overall $CO_2$

electrolysis.[60,61] H-type cells are widely employed in various electrochemical reactions due to their simple and cost-effective setup. However, the low $CO_2$ solubility in aqueous solution (~34 mM under ambient conditions) and the slow $CO_2$ diffusion limit the mass transfer efficiency over the electrode, leading to inferior current density. Moreover, the excessive supply of $H_2O$ and insufficient supply of $CO_2$ over the immersed electrode are unfavoured for the $sCO_2RR$ to multi-carbon products (denoted as $C_{2+}$, *i.e.*, $C_2H_4$ and $C_2H_5OH$) as high concentrations of $CO_2$ or CO intermediates are preferred for the C–C coupling process.[62–64] Besides, the long distance between the anode and the cathode inevitably results in a pronounced voltage drop due to the high resistance.

Compared with H-type cells, flow cells enable efficient mass-transfer for industrial-scale current density owing to the high-quality catalyst-electrolyte-gas tri-phase interface and the continuous electrolyte/gas flow (Fig. 8a).[65] Different from H-type cells, a gas diffusion electrode consisting of a hydrophobic gas diffusion layer (GDL) and catalyst layer is required. Gaseous $CO_2$ can efficiently diffuse across the GDL to the catalyst layer to meet the catholyte, thereby forming the above-mentioned tri-phase interface for the enhanced $CO_2RR$. The flowing anolyte also promotes the removal of products and attached bubbles and facilitates mass transfer near the anode, thereby enhancing the anodic reaction rate. However, flow cells also show drawbacks. The hydrophobic surface of the GDE gradually becomes hydrophilic during high-current electrolysis, which leads to catholyte flooding and gas feed blocking. Besides, the commonly used carbon paper to fabricate GDL is broken easily in the electrolyte/gas flow due to its weak mechanical strength. To alleviate these issues, Dinh *et al.* reported a polytetrafluoroethylene (PTFE)/Cu/carbon nanoparticles/graphite composite GDE which could run for 150 h with the $C_2H_4$ FE maintained over 60%.[64] In sharp contrast, the $C_2H_4$ FE rapidly dropped to 10% within 1 h for the conventional carbon paper/Cu GDE. The robust PTFE with a hydrophobic surface effectively prevented flooding, and the carbon nanoparticles and graphite layer stabilized the Cu catalyst surface.

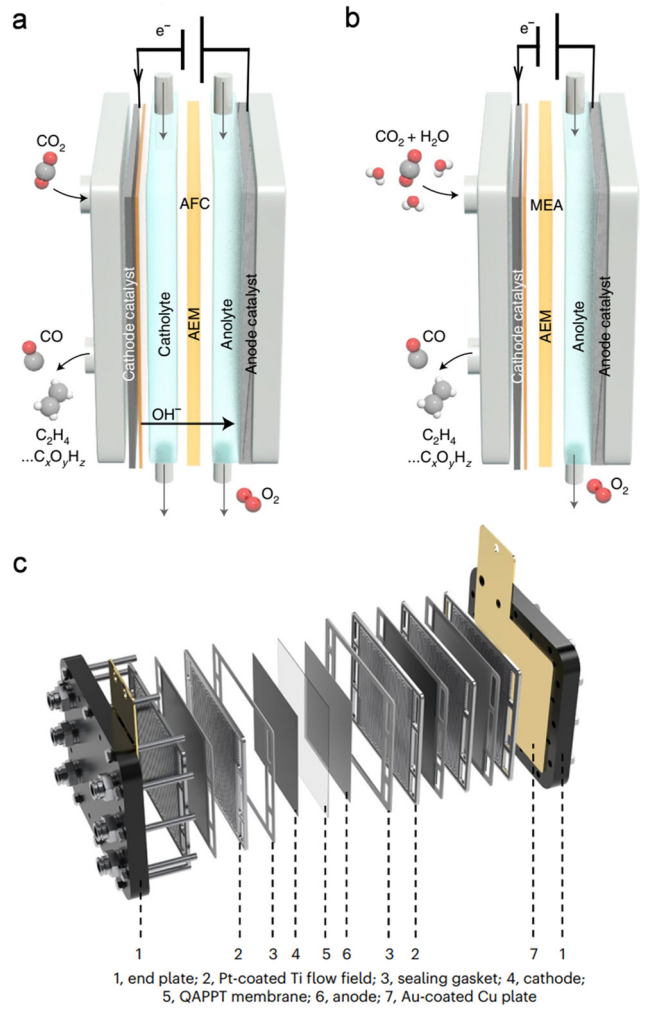


Fig. 8 Schematic of (a) an alkaline electrolyte flow cell (AFC) and (b) an MEA electrolyser. Reproduced with permission from ref. 65. Copyright 2022, Springer Nature. (c) Scale-up electrolyser stack with four 10 × 10 $cm^2$ MEAs. Reproduced with permission from ref. 67. Copyright 2023, Springer Nature.

A catholyte-free MEA electrolyser provides a solution to prevent the flooding issue (Fig. 8b).[65,66] Moreover, the closely packed cathode–membrane–anode structure of the MEA minimizes the electricity resistance for enhanced energy efficiency. Zhou *et al.* reported that in a flow cell, the $CO_2RR$-MOR required 2.74 V to deliver a current density of 100 mA $cm^{-2}$, whereas a high current density approaching 500 mA $cm^{-2}$ was achieved at merely 2.4 V in an MEA electrolyser.[18] This is especially important for a scale-up stack where several MEAs are integrated. An electrolyser stack with four 10 × 10 $cm^2$ MEAs was successfully constructed for scale-up $CO_2$ electrolysis by Bao's group (Fig. 8c).[67] Impressively, a current of 60 A was achieved with a $C_{2+}$ FE of over 80% at a cell voltage of ~13.5 V, and the current could be further increased to 150 A with nearly 90% $C_{2+}$ FE at a cell voltage less than 11 V when fed with CO. Such a scale-up device provides an appealing way for practical utilization of $CO_2$ electrolysis, and further improvements are required to couple the $CO_2RR$ with various value-added anodic reactions in the future.

In addition to the electrolyser architecture, the electrolyte also plays a pivotal role in electrolysis. An alkaline solution is employed in many $CO_2RR$ cases owing to the low ohmic resistance and effective suppression of the HER. However, severe $CO_2$ loss (75–95%) occurs under these conditions due to the rapid reaction of $CO_2$ with alkali to form carbonate and bicarbonate (Fig. 9), and the regeneration of the alkaline electrolyte accounts for 60–75% of total energy consumption.[65] Moreover, $CO_2RR$ products such as formate can diffuse across the anion exchange membrane to the anodic part, leading to difficulties in product collection and separation. Therefore, the acidic $CO_2RR$ seems attractive. Unfortunately, most of the alternative anodic reactions such as $CH_3OH$, glycerol, and HMF oxidation are kinetically favourable in alkaline electrolytes. To deal with the above issues, a bipolar membrane was adopted.[17] Nevertheless, the sluggish water dissociation into $H^+$ and $OH^-$ inside the bipolar membrane

 

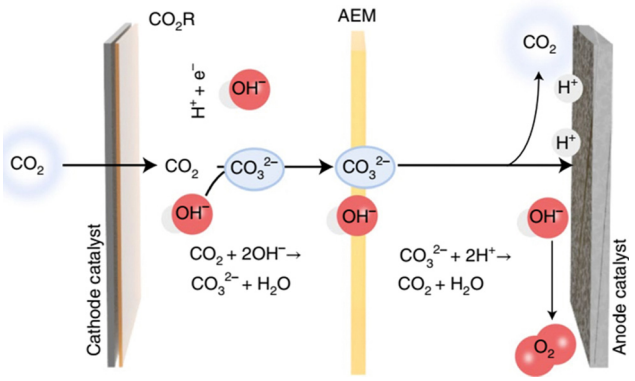


Fig. 9 $CO_2$ loss *via* carbonate formation and crossover to the anodic side under alkaline conditions. Reproduced with permission from ref. 65. Copyright 2022, Springer Nature.

as well as the increased membrane thickness leads to extra voltage loss compared with an AEM or cation exchange membrane (CEM). In addition, the higher expense of the bipolar membrane also hinders its application.

### 3.3. Development of an electrocatalyst under acidic conditions

As mentioned above, overall $CO_2$ electrolysis in acidic electrolytes can address the issue of $CO_2$ loss for improved energy efficiency. Although performing the $CO_2$RR under acidic conditions is preferred, and indeed improved performances were obtained for the acidic $CO_2$RR by controlling the catalyst surface microenvironments,[68–72] few catalysts have shown promising activity for the alternative anodic reactions in acidic anolyte. In fact, the hydroxyl group (*OH) plays a pivotal role in the dehydrogenation processes of the anodic oxidation reactions, the formation of which is hindered due to the acidic conditions.[73] Moreover, operation at the positive potential in an acidic solution will cause rapid decomposition of the non-noble metal anode, resulting in poor stability. A recent work presented an electrocatalyst featuring $MnO_2$ nanosheets for the acidic GOR.[74] A long-term steady electrolysis of over 800 h was achieved at 10 mA $cm^{-2}$ in 0.2 M glycerol + 0.005 M $H_2SO_4$. However, both formate and $CO_2$ were obtained with close FEs (~50% for each), indicating the easy overoxidation of glycerol under acidic conditions. Therefore, developing highly acid-tolerant electrocatalysts with enhanced activity and selectivity remains a great challenge, and demands further investigations.

### 3.4. Selectivity control for target products

It is quite challenging to control the selectivity of certain products for anodic organic oxidations. For instance, in alcohol oxidations, the C–OH group easily gets oxidized to –COOH rather than –CHO. Therefore, partial oxidation of alcohol to aldehyde is difficult. It becomes more challenging to selectively produce intermediate chemicals when there are more than one reductive group in the reactant molecule. For the HMFOR, owing to the coexistence of –CHO and $–CH_2OH$ groups in an HMF molecule, the oxidation of HMF to FDCA can proceed *via* HMFCA or DFF (Fig. 6). However, given the widely-used alkaline electrolyte for the HMFOR in the $CO_2$RR-HMFOR couple, the HMFCA pathway is usually preferred and thus it is difficult to obtain DFF in such a coupling system.[46] Besides, C–C bond breaking may occur under harsh conditions for multi-carbon molecules, increasing the variety of products.[19] Moreover, over-oxidation of organic molecules to $CO_2$ was also observed at high potentials/current densities. For example, quite an amount of $CO_2$ can be generated during the MOR on Pt and $IrO_2$ catalysts at ~100 mA $cm^{-2}$.[15] Simultaneously achieving high current density and selectivity in these alternative organic oxidation reactions remains challenging. As for the cathodic side, although most works show no significant change in the selectivity of the $CO_2$RR when the $CO_2$RR is coupled with alternative anodic oxidation reactions, sometimes the organic molecules may cross the ion-exchange membrane to the cathodic side and influence the $CO_2$RR process.

## 4. Conclusions and perspectives

Coupling $CO_2$RR to various anodic oxidation reactions with value-added products provides a novel avenue for enhancing the economic output of overall $CO_2$ electrolysis. In this review, a series of oxidation reactions have been discussed as competing alternatives to the OER with reference to the latest advances. We have also pointed out the major challenges in achieving efficient overall $CO_2$ electrolysis with alternative anodic reactions. Despite the pronounced advancement made in the coupling strategy, this field is still nascent.

The design of efficient electrocatalysts requires an in-depth understanding of the mechanisms, which largely relies on advanced characterization studies and theoretical simulations.[75] Recently, *in situ* infrared spectroscopy, X-ray photoelectron spectroscopy (XPS), X-ray absorption fine structure spectroscopy and other techniques have been adopted in many works, providing useful local information about reaction intermediates. However, given the complex microenvironment over the catalyst's surface during the reaction, detecting the evolution of active sites and intermediates under working conditions using operando characterization is crucial to uncover the true reaction pathways, which is still difficult owing to the harsh conditions such as high vacuum for XPS and the severe decay and disturbance of signals by the electrolyte for infrared spectroscopy.[76,77] The design of electrolysers that are compatible to various operando and time-resolved characterization studies is in urgent demand.

As for theoretical simulation, the accuracy of the model directly influences the calculation result, which is, however, extremely challenging in heterogeneous electrocatalysis considering the interfacial diversity. The structures of active sites are not uniform over the catalyst surface. Moreover, the active sites may evolve during catalysis, making it more difficult to obtain accurate surface structures for the simulation. Besides, the electrolyte near the electrode should also be taken into account in the simulation. The ion concentration and solvation

effect may influence the adsorption of intermediates, thus leading to different calculation results. Obviously, combining advanced calculation methods with operando characterization holds the key to deciphering the in-depth reaction mechanisms, and therefore benefits the development of high-performance electrocatalysts.

Beyond the catalysts, the overall design of the whole electrolysis system is also crucial, which has not received enough attention currently. For electrolysers, the flow fields for both the anode and cathode should be specially designed to achieve efficient mass transfer. Besides, the feeding rates for $CO_2$ and anodic reactants should be well adjusted to optimize the total conversion rates. In addition, for industrial applications, the feeding, collecting, and recycling systems should match with each other for steady operation. A well-established overall $CO_2$ electrolysis system with comprehensive technoeconomic evaluations requires scientists from various backgrounds including chemistry, materials science, physics, engineering, economics, *etc.* It is expected that continuous efforts will propel this technique to industrial application in the near future.

## Author contributions

Y. L. and T. L. supervised the project. Y. L. wrote the manuscript.

## Conflicts of interest

There are no conflicts to declare.

## Acknowledgements

This work was supported by the National Key R & D Program of China (2017YFA0700104), the National Natural Science Foundation of China (21905204 and 21931007), and the 111 Project of China (D17003).

## References

1 C. Chen, J. F. Khosrowabadi Kotyk and S. W. Sheehan, Progress toward commercial application of electrochemical carbon dioxide reduction, *Chem*, 2018, **4**, 2571–2586.
2 R. Francke, B. Schille and M. Roemelt, Homogeneously catalyzed electroreduction of carbon dioxide—methods, mechanisms, and catalysts, *Chem. Rev.*, 2018, **118**, 4631–4701.
3 P. Zhu, C. Xia, C.-Y. Liu, K. Jiang, G. Gao, X. Zhang, Y. Xia, Y. Lei, H. N. Alshareef, T. P. Senftle and H. Wang, Direct and continuous generation of pure acetic acid solutions via electrocatalytic carbon monoxide reduction, *Proc. Natl. Acad. Sci. U. S. A.*, 2021, **118**, e2010868118.
4 J. Gu, C.-S. Hsu, L. Bai, H. M. Chen and X. Hu, Atomically dispersed Fe3+ sites catalyze efficient CO2 electroreduction to CO, *Science*, 2019, **364**, 1091–1094.
5 J. Na, B. Seo, J. Kim, C. W. Lee, H. Lee, Y. J. Hwang, B. K. Min, D. K. Lee, H.-S. Oh and U. Lee, General techno-economic analysis for electrochemical coproduction coupling carbon dioxide reduction with organic oxidation, *Nat. Commun.*, 2019, **10**, 5193.
6 M.-Y. Qi, M. Conte, M. Anpo, Z.-R. Tang and Y.-J. Xu, Cooperative coupling of oxidative organic synthesis and hydrogen production over semiconductor-based photocatalysts, *Chem. Rev.*, 2021, **121**, 13051–13085.
7 L. Yuan, M.-Y. Qi, Z.-R. Tang and Y.-J. Xu, Coupling strategy for $CO_2$ valorization integrated with organic synthesis by heterogeneous photocatalysis, *Angew. Chem., Int. Ed.*, 2021, **60**, 21150–21172.
8 M.-Y. Qi, M. Conte, Z.-R. Tang and Y.-J. Xu, Engineering semiconductor quantum dots for selectivity switch on high-performance heterogeneous coupling photosynthesis, *ACS Nano*, 2022, **16**, 17444–17453.
9 F.-K. Shang, Y.-H. Li, M.-Y. Qi, Z.-R. Tang and Y.-J. Xu, Photocatalytic materials for sustainable chemistry via cooperative photoredox catalysis, *Catal. Today*, 2023, **410**, 85–101.
10 Y. Zhu, J. Zhang, Q. Qian, Y. Li, Z. Li, Y. Liu, C. Xiao, G. Zhang and Y. Xie, Dual nanoislands on Ni/C hybrid nanosheet activate superior hydrazine oxidation-assisted high-efficiency $H_2$ production, *Angew. Chem., Int. Ed.*, 2022, **61**, e202113082.
11 L. Zhu, J. Huang, G. Meng, T. Wu, C. Chen, H. Tian, Y. Chen, F. Kong, Z. Chang, X. Cui and J. Shi, Active site recovery and N-N bond breakage during hydrazine oxidation boosting the electrochemical hydrogen production, *Nat. Commun.*, 2023, **14**, 1997.
12 H. Jiang, M. Sun, S. Wu, B. Huang, C.-S. Lee and W. Zhang, Oxygen-incorporated NiMoP nanotube arrays as efficient bifunctional electrocatalysts for urea-assisted energy-saving hydrogen production in alkaline electrolyte, *Adv. Funct. Mater.*, 2021, **31**, 2104951.
13 S.-S. Liu, Q.-J. Xing, Y. Chen, M. Zhu, X.-H. Jiang, S.-H. Wu, W. Dai and J.-P. Zou, Photoelectrochemical degradation of organic pollutants using BiOBr anode coupled with simultaneous $CO_2$ reduction to liquid fuels via CuO cathode, *ACS Sustainable Chem. Eng.*, 2019, **7**, 1250–1259.
14 Q. Wang, C. Zhu, C. Wu and H. Yu, Direct synthesis of bismuth nanosheets on a gas diffusion layer as a high-performance cathode for a coupled electrochemical system capable of electroreduction of $CO_2$ to formate with simultaneous degradation of organic pollutants, *Electrochim. Acta*, 2019, **319**, 138–147.
15 Y. Li, C.-Z. Huo, H.-J. Wang, Z.-X. Ye, P.-P. Luo, X.-X. Cao and T.-B. Lu, Coupling $CO_2$ reduction with $CH_3OH$ oxidation for efficient electrosynthesis of formate on hierarchical bifunctional CuSn alloy, *Nano Energy*, 2022, **98**, 107277.
16 X. Wei, Y. Li, L. Chen and J. Shi, Formic acid electro-synthesis by concurrent cathodic $CO_2$ reduction and anodic $CH_3OH$ oxidation, *Angew. Chem., Int. Ed.*, 2021, **60**, 3148–3155.
17 C. Cao, D.-D. Ma, J. Jia, Q. Xu, X.-T. Wu and Q.-L. Zhu, Divergent paths, same goal: a pair-electrosynthesis tactic for

 

cost-efficient and exclusive formate production by metal–organic-framework-derived 2D electrocatalysts, *Adv. Mater.*, 2021, **33**, 2008631.

18 Y. Zhou, Z. Wang, W. Fang, R. Qi, Z. Wang, C. Xia, K. Lei, B. You, X. Yang, Y. Liu, W. Guo, Y. Su, S. Ding and B. Y. Xia, Modulating O–H activation of methanol oxidation on nickel-organic frameworks for overall CO2 electrolysis, *ACS Catal.*, 2023, **13**, 2039–2046.

19 J. Bi, Q. Zhu, W. Guo, P. Li, S. Jia, J. Liu, J. Ma, J. Zhang, Z. Liu and B. Han, Simultaneous $CO_2$ reduction and 5-hydroxymethylfurfural oxidation to value-added products by electrocatalysis, *ACS Sustainable Chem. Eng.*, 2022, **10**, 8043–8050.

20 Y. Liang, W. Zhou, Y. Shi, C. Liu and B. Zhang, Unveiling in situ evolved $In/In_2O_{3-x}$ heterostructure as the active phase of $In_2O_3$ toward efficient electroreduction of $CO_2$ to formate, *Sci. Bull.*, 2020, **65**, 1547–1554.

21 T. Wang, X. Cao and L. Jiao, Progress in hydrogen production coupled with electrochemical oxidation of small molecules, *Angew. Chem., Int. Ed.*, 2022, **61**, e202213328.

22 J. Jack, W. Zhu, J. L. Avalos, J. Gong and Z. J. Ren, Anode co-valorization for scalable and sustainable electrolysis, *Green Chem.*, 2021, **23**, 7917–7936.

23 L. Chen and J. Shi, Co-electrolysis toward value-added chemicals, *Sci. China Mater.*, 2022, **65**, 1–9.

24 S. A. Lee, M. G. Lee and H. W. Jang, Catalysts for electrochemical ammonia oxidation: Trend, challenge, and promise, *Sci. China Mater.*, 2022, **65**, 3334–3352.

25 K. Siddharth, Y. Hong, X. Qin, H. J. Lee, Y. T. Chan, S. Zhu, G. Chen, S.-I. Choi and M. Shao, Surface engineering in improving activity of Pt nanocubes for ammonia electrooxidation reaction, *Appl. Catal., B*, 2020, **269**, 118821.

26 M. J. Trenerry, C. M. Wallen, T. R. Brown, S. V. Park and J. F. Berry, Spontaneous $N_2$ formation by a diruthenium complex enables electrocatalytic and aerobic oxidation of ammonia, *Nat. Chem.*, 2021, **13**, 1221–1227.

27 W. Xu, D. Du, R. Lan, J. Humphreys, D. N. Miller, M. Walker, Z. Wu, J. T. S. Irvine and S. Tao, Electrodeposited NiCu bimetal on carbon paper as stable non-noble anode for efficient electrooxidation of ammonia, *Appl. Catal., B*, 2018, **237**, 1101–1109.

28 F. Almomani, R. Bhosale, M. Khraisheh, A. Kumar and M. Tawalbeh, Electrochemical oxidation of ammonia on nickel oxide nanoparticles, *Int. J. Hydrogen Energy*, 2020, **45**, 10398–10408.

29 X. V. Medvedeva, J. J. Medvedev, S. W. Tatarchuk, R. M. Choueiri and A. Klinkova, Sustainable at both ends: electrochemical $CO_2$ utilization paired with electrochemical treatment of nitrogenous waste, *Green Chem.*, 2020, **22**, 4456–4462.

30 M. Choi, J. W. Kim, S. Chung, Y. Lee, S. Bong and J. Lee, Syngas production for Fischer-Tropsch process via co-electrolytic processes of $CO_2$ reduction and $NH_3$ oxidation, *Chem. Eng. J.*, 2022, **430**, 132563.

31 X. Wang, J.-P. Li, Y. Duan, J. Li, H. Wang, X. Yang and M. Gong, Electrochemical urea oxidation in different environment: From mechanism to devices, *ChemCatChem*, 2022, **14**, e202101906.

32 R. Clark, A. Moore, M. MacInnis and E. Bertin, Investigation of urea oxidation as a potential anode reaction during $CO_2$ electrolysis, *J. Appl. Electrochem.*, 2021, **51**, 1583–1590.

33 J.-H. Guo and W.-Y. Sun, Integrating nickel-nitrogen doped carbon catalyzed CO2 electroreduction with chlor-alkali process for CO, Cl2 and KHCO3 production with enhanced techno-economics, *Appl. Catal., B*, 2020, **275**, 119154.

34 R. Ge, L.-Y. Dong, X. Hu, Y.-T. Wu, L. He, G.-P. Hao and A.-H. Lu, Intensified coupled electrolysis of $CO_2$ and brine over electrocatalysts with ordered mesoporous transport channels, *Chem. Eng. J.*, 2022, **438**, 135500.

35 X. Tan, C. Yu, X. Song, C. Zhao, S. Cui, H. Xu, J. Chang, W. Guo, Z. Wang, Y. Xie and J. Qiu, Toward an understanding of the enhanced $CO_2$ electroreduction in NaCl electrolyte over CoPc molecule-implanted graphitic carbon nitride catalyst, *Adv. Energy Mater.*, 2021, **11**, 2100075.

36 L. Fan, X. Bai, C. Xia, X. Zhang, X. Zhao, Y. Xia, Z.-Y. Wu, Y. Lu, Y. Liu and H. Wang, $CO_2$/carbonate-mediated electrochemical water oxidation to hydrogen peroxide, *Nat. Commun.*, 2022, **13**, 2668.

37 S.-N. Sun, L.-Z. Dong, J.-R. Li, J.-W. Shi, J. Liu, Y.-R. Wang, Q. Huang and Y.-Q. Lan, Redox-active crystalline coordination catalyst for hybrid electrocatalytic methanol oxidation and $CO_2$ reduction, *Angew. Chem., Int. Ed.*, 2022, **61**, e202207282.

38 S. Verma, S. Lu and P. J. A. Kenis, Co-electrolysis of $CO_2$ and glycerol as a pathway to carbon chemicals with improved technoeconomics due to low electricity consumption, *Nat. Energy*, 2019, **4**, 466–474.

39 K. Fernández-Caso, A. Peña-Rodríguez, J. Solla-Gullón, V. Montiel, G. Díaz-Sainz, M. Alvarez-Guerra and A. Irabien, Continuous carbon dioxide electroreduction to formate coupled with the single-pass glycerol oxidation to high value-added products, *J. CO2 Util.*, 2023, **70**, 102431.

40 G. Wang, J. Chen, K. Li, J. Huang, Y. Huang, Y. Liu, X. Hu, B. Zhao, L. Yi, T. W. Jones and Z. Wen, Cost-effective and durable electrocatalysts for Co-electrolysis of $CO_2$ conversion and glycerol upgrading, *Nano Energy*, 2022, **92**, 106751.

41 M. A. Bajada, S. Roy, J. Warnan, K. Abdiaziz, A. Wagner, M. M. Roessler and E. Reisner, A precious-metal-free hybrid electrolyzer for alcohol oxidation coupled to $CO_2$-to-syngas conversion, *Angew. Chem., Int. Ed.*, 2020, **59**, 15633–15641.

42 G. Yang, Y. Jiao, H. Yan, Y. Xie, A. Wu, X. Dong, D. Guo, C. Tian and H. Fu, Interfacial engineering of $MoO_2$-FeP heterojunction for highly efficient hydrogen evolution coupled with biomass electrooxidation, *Adv. Mater.*, 2020, **32**, 2000455.

43 P. Prabhu, Y. Wan and J.-M. Lee, Electrochemical conversion of biomass derived products into high-value chemicals, *Matter*, 2020, **3**, 1162–1177.

44 K. Gu, D. Wang, C. Xie, T. Wang, G. Huang, Y. Liu, Y. Zou, L. Tao and S. Wang, Defect-rich high-entropy oxide nanosheets for efficient 5-hydroxymethylfurfural electrooxidation, *Angew. Chem., Int. Ed.*, 2021, **60**, 20253–20258.

45 R. Ge, Y. Wang, Z. Li, M. Xu, S.-M. Xu, H. Zhou, K. Ji, F. Chen, J. Zhou and H. Duan, Selective electrooxidation of biomass-derived alcohols to aldehydes in a neutral medium: Promoted water dissociation over a nickel-oxide-supported ruthenium single-atom catalyst, *Angew. Chem., Int. Ed.*, 2022, **61**, e202200211.
46 Y. Yang and T. Mu, Electrochemical oxidation of biomass derived 5-hydroxymethylfurfural (HMF): pathway, mechanism, catalysts and coupling reactions, *Green Chem.*, 2021, **23**, 4228–4254.
47 N. Zhang, Y. Zou, L. Tao, W. Chen, L. Zhou, Z. Liu, B. Zhou, G. Huang, H. Lin and S. Wang, Electrochemical oxidation of 5-hydroxymethylfurfural on nickel nitride/carbon nanosheets: Reaction pathway determined by in situ sum frequency generation vibrational spectroscopy, *Angew. Chem., Int. Ed.*, 2019, **58**, 15895–15903.
48 Y. Lu, T. Liu, Y.-C. Huang, L. Zhou, Y. Li, W. Chen, L. Yang, B. Zhou, Y. Wu, Z. Kong, Z. Huang, Y. Li, C.-L. Dong, S. Wang and Y. Zou, Integrated catalytic sites for highly efficient electrochemical oxidation of the aldehyde and hydroxyl groups in 5-hydroxymethylfurfural, *ACS Catal.*, 2022, **12**, 4242–4251.
49 K. Yang, N. Zhang, J. Yang, Z. Xu, J. Yan, D. Li and S. Liu, Synergistic marriage of $CO_2$ reduction and sulfide oxidation towards a sustainable co-electrolysis process, *Appl. Catal., B*, 2023, **332**, 122718.
50 J. C. Fornaciari, D. Primc, K. Kawashima, B. R. Wygant, S. Verma, L. Spanu, C. B. Mullins, A. T. Bell and A. Z. Weber, A perspective on the electrochemical oxidation of methane to methanol in membrane electrode assemblies, *ACS Energy Lett.*, 2020, **5**, 2954–2963.
51 E. Sargeant, A. Kolodziej, C. S. Le Duff and P. Rodriguez, Electrochemical conversion of $CO_2$ and $CH_4$ at subzero temperatures, *ACS Catal.*, 2020, **10**, 7464–7474.
52 J. Lu, C. Zhu, C. Pan, W. Lin, J. P. Lemmon, F. Chen, C. Li and K. Xie, Highly efficient electrochemical reforming of $CH_4/CO_2$ in a solid oxide electrolyser, *Sci. Adv.*, 2018, **4**, eaar5110.
53 T. Tan, W. Wang, K. Zhang, Z. Zhan, W. Deng, Q. Zhang and Y. Wang, Upcycling plastic wastes into value-added products by heterogeneous catalysis, *ChemSusChem*, 2022, **15**, e202200522.
54 X. Du, H. Zhang, K. P. Sullivan, P. Gogoi and Y. Deng, Electrochemical lignin conversion, *ChemSusChem*, 2020, **13**, 4318–4343.
55 H. Zhao, D. Lu, J. Wang, W. Tu, D. Wu, S. W. Koh, P. Gao, Z. J. Xu, S. Deng, Y. Zhou, B. You and H. Li, Raw biomass electroreforming coupled to green hydrogen generation, *Nat. Commun.*, 2021, **12**, 2008.
56 X. Du, W. Liu, Z. Zhang, A. Mulyadi, A. Brittain, J. Gong and Y. Deng, Low-energy catalytic electrolysis for simultaneous hydrogen evolution and lignin depolymerization, *ChemSusChem*, 2017, **10**, 847–854.
57 F.-Y. Chen, Z.-Y. Wu, S. Gupta, D. J. Rivera, S. V. Lambeets, S. Pecaut, J. Y. T. Kim, P. Zhu, Y. Z. Finfrock, D. M. Meira, G. King, G. Gao, W. Xu, D. A. Cullen, H. Zhou, Y. Han, D. E. Perea, C. L. Muhich and H. Wang, Efficient conversion of low-concentration nitrate sources into ammonia on a Ru-dispersed Cu nanowire electrocatalyst, *Nat. Nanotechnol.*, 2022, **17**, 759–767.
58 G. Lee, Y. C. Li, J.-Y. Kim, T. Peng, D.-H. Nam, A. Sedighian Rasouli, F. Li, M. Luo, A. H. Ip, Y.-C. Joo and E. H. Sargent, Electrochemical upgrade of $CO_2$ from amine capture solution, *Nat. Energy*, 2021, **6**, 46–53.
59 I. Sullivan, A. Goryachev, I. A. Digdaya, X. Li, H. A. Atwater, D. A. Vermaas and C. Xiang, Coupling electrochemical $CO_2$ conversion with $CO_2$ capture, *Nat. Catal.*, 2021, **4**, 952–958.
60 D. M. Weekes, D. A. Salvatore, A. Reyes, A. Huang and C. P. Berlinguette, Electrolytic $CO_2$ reduction in a flow cell, *Acc. Chem. Res.*, 2018, **51**, 910–918.
61 S. Liang, N. Altaf, L. Huang, Y. Gao and Q. Wang, Electrolytic cell design for electrochemical $CO_2$ reduction, *J. CO2 Util.*, 2020, **35**, 90–105.
62 J. Li, G. Chen, Y. Zhu, Z. Liang, A. Pei, C.-L. Wu, H. Wang, H. R. Lee, K. Liu, S. Chu and Y. Cui, Efficient electrocatalytic $CO_2$ reduction on a three-phase interface, *Nat. Catal.*, 2018, **1**, 592–600.
63 T.-T. Zhuang, Z.-Q. Liang, A. Seifitokaldani, Y. Li, P. De Luna, T. Burdyny, F. Che, F. Meng, Y. Min, R. Quintero-Bermudez, C. T. Dinh, Y. Pang, M. Zhong, B. Zhang, J. Li, P.-N. Chen, X.-L. Zheng, H. Liang, W.-N. Ge, B.-J. Ye, D. Sinton, S.-H. Yu and E. H. Sargent, Steering post-C–C coupling selectivity enables high efficiency electroreduction of carbon dioxide to multi-carbon alcohols, *Nat. Catal.*, 2018, **1**, 421–428.
64 C.-T. Dinh, T. Burdyny, M. G. Kibria, A. Seifitokaldani, C. M. Gabardo, F. P. García de Arquer, A. Kiani, J. P. Edwards, P. De Luna, O. S. Bushuyev, C. Zou, R. Quintero-Bermudez, Y. Pang, D. Sinton and E. H. Sargent, $CO_2$ electroreduction to ethylene via hydroxide-mediated copper catalysis at an abrupt interface, *Science*, 2018, **360**, 783–787.
65 A. Ozden, F. P. García de Arquer, J. E. Huang, J. Wicks, J. Sisler, R. K. Miao, C. P. O'Brien, G. Lee, X. Wang, A. H. Ip, E. H. Sargent and D. Sinton, Carbon-efficient carbon dioxide electrolysers, *Nat. Sustainable*, 2022, **5**, 563–573.
66 T. Zheng, K. Jiang, N. Ta, Y. Hu, J. Zeng, J. Liu and H. Wang, Large-scale and highly selective $CO_2$ electrocatalytic reduction on nickel single-atom catalyst, *Joule*, 2019, **3**, 265–278.
67 P. Wei, D. Gao, T. Liu, H. Li, J. Sang, C. Wang, R. Cai, G. Wang and X. Bao, Coverage-driven selectivity switch from ethylene to acetate in high-rate $CO_2$/CO electrolysis, *Nat. Nanotechnol.*, 2023, **18**, 299–306.
68 M. C. O. Monteiro, M. F. Philips, K. J. P. Schouten and M. T. M. Koper, Efficiency and selectivity of $CO_2$ reduction to CO on gold gas diffusion electrodes in acidic media, *Nat. Commun.*, 2021, **12**, 4943.
69 Y. Xie, P. Ou, X. Wang, Z. Xu, Y. C. Li, Z. Wang, J. E. Huang, J. Wicks, C. McCallum, N. Wang, Y. Wang, T. Chen, B. T. W. Lo, D. Sinton, J. C. Yu, Y. Wang and E. H. Sargent, High carbon utilization in CO2 reduction to multi-carbon products in acidic media, *Nat. Catal.*, 2022, **5**, 564–570.

 

70 J. Gu, S. Liu, W. Ni, W. Ren, S. Haussener and X. Hu, Modulating electric field distribution by alkali cations for $CO_2$ electroreduction in strongly acidic medium, *Nat. Catal.*, 2022, **5**, 268–276.
71 J. E. Huang, F. Li, A. Ozden, A. Sedighian Rasouli, F. P. García de Arquer, S. Liu, S. Zhang, M. Luo, X. Wang, Y. Lum, Y. Xu, K. Bertens, R. K. Miao, C.-T. Dinh, D. Sinton and E. H. Sargent, $CO_2$ electrolysis to multicarbon products in strong acid, *Science*, 2021, **372**, 1074–1078.
72 Y. Zhao, L. Hao, A. Ozden, S. Liu, R. K. Miao, P. Ou, T. Alkayyali, S. Zhang, J. Ning, Y. Liang, Y. Xu, M. Fan, Y. Chen, J. E. Huang, K. Xie, J. Zhang, C. P. O'Brien, F. Li, E. H. Sargent and D. Sinton, Conversion of $CO_2$ to multicarbon products in strong acid by controlling the catalyst microenvironment, *Nat. Synth.*, 2023, **2**, 403–412.
73 T. Iwasita, Electrocatalysis of methanol oxidation, *Electrochim. Acta*, 2002, **47**, 3663–3674.
74 Y. Li, X. Wei, S. Han, L. Chen and J. Shi, $MnO_2$ electrocatalysts coordinating alcohol oxidation for ultra-durable hydrogen and chemical productions in acidic solutions, *Angew. Chem., Int. Ed.*, 2021, **60**, 21464–21472.
75 L. Li, Y. Sun and Y. Xie, Catalysts design for $CO_2$ electroreduction, *Sci. China: Chem.*, 2022, **65**, 425–427.
76 Q. Liu, X.-G. Zhang, Z.-Y. Du, C.-J. Zou, H.-Y. Chen, Y. Zhao, J.-C. Dong, P.-P. Fang and J.-F. Li, Converting $CO_2$ to ethanol on Ag nanowires with high selectivity investigated by operando Raman spectroscopy, *Sci. China: Chem.*, 2023, **66**, 259–265.
77 X. Song, L. Xu, X. Sun and B. Han, In situ/operando characterization techniques for electrochemical CO2 reduction, *Sci. China Chem.*, 2023, **66**, 315–323.